Vol. XX, Nº 1, Junio (2012)
Matemáticas: 3–19

Matemáticas:
Enseñanza Universitaria

ZAD strategy with lateral PWM applied to a Boost converter

Andrés Amador
Pontificia Universidad Javeriana Cali

Simeon Casanova
Universidad Nacional de Colombia

Julián Hurtado
Universidad Autónoma de Occidente

Gerard Olivar
Universidad Nacional de Colombia

Received Apr. 08, 2011 Accepted Feb. 10, 2012

Abstract

In this paper we show some results about the dynamics of a Boost converter when it is controlled by lateral PWM (Pulse Width Modulator) and ZAD (Zero Average Dynamics) strategy. Different nonlinear phenomena like bifurcations and chaos are reported when the parameters associated to the system are varied. Finally, chaos present in the converter is controlled using FPIC (Fixed Point Induced Control) and TDAS (Time-Delay Autosynchronization) techniques.

Keywords: Boost converter, ZAD, duty cycle, bifurcations, chaos control.

MSC(2000): 93B12, 34C23, 37D45

1 Introduction

Nonlinear phenomena in power electronics (including bifurcations and chaos) has been reported in [1, 2, 3, 4, 5, 6, 7, 8, 9]. Boost converters are one of the most widely used circuits in Power Electronics. One of its main drawbacks occurring in the design of this converter is the stability of the system to input and output disturbances. For this reason it is necessary to understand the dynamics, specially when some parameters are varied. In the last decades several papers on the dynamics of Buck, Boost and Buck-Boost converters with different control techniques have appeared [10, 11, 12, 13, 14, 15, 16, 17, 18, 19] but no one reports a study on the dynamics of a Boost converter with ZAD strategy. The benefits of the ZAD strategy include simplicity and practicality. The ZAD controller yields a converter performance more robust than those usually obtained by PID (proportional-integral-derivative) controllers, specifically with respect to nonlinear loads. It involves the direct design of the duty cycle and is implemented in a single updated lateral PWM [20]. In [21], ZAD strategy control is used in a Buck converter and an analysis of stability and transition to chaos is studied. ZAD control scheme, proposed in [22], tries to conjugate the advantages of fixed frequency implementations and the inherent robustness of sliding control modes. It is based on an appropriate design of the output that guarantees the fulfillment of the specifications and on a specific design of the PWM duty cycle in such a way that the output average in each PWM-period is zero. Due to the existence of chaotic behavior in the boost converter with this ZAD scheme, among

others [23] some chaos control techniques known as TDAS [24, 3, 25] and FPIC [21, 25, 26, 27, 28] have been designed.

The rest of the paper is outlined as follows. Section 2 is devoted to the basic description of the dynamical model to the boost converter driven with a PWM lateral pulse and ZAD strategy. In Section 3 one-parameter bifurcation diagrams are derived numerically using MATLAB. Section 4 and 5 deal with the performance of chaos control techniques in the boost converter. Namely FPIC in section 4 and TDAS in section 5. Conclusions in section 6 end this paper.

2 Boost converter with ZAD strategy

In this section we introduce the DC/DC boost converter with ZAD strategy. The dynamics of a Boost converter is controlled by the solutions of the following differential equations system

$$\begin{aligned} \frac{dv}{d\tau} &= -\frac{1}{RC}v + (1-u)\frac{1}{C}i \\ \frac{di}{d\tau} &= -(1-u)\frac{1}{L}v + \frac{V_{in}}{L} \end{aligned} \tag{1}$$

here the control input u takes discrete values in the set $\{0, 1\}$ corresponding to the lateral PWM case. Parameter values are chosen as, $R = 20\,\Omega$, $C = 40\,\mu F$, $L = 2\,mH$, $V_{in} = 40\,V$ and $T_c = 50\,\mu s$ (corresponding to sampling period). Also, we consider the voltage v on the capacitor and the current i on the inductor as the state variables.

The system (1) becomes nondimensional (eq. (2)) after a simple change of variables given by [29]

$$x_1 = \frac{v}{V_{in}}, \quad x_2 = \frac{i}{V_{in}}\sqrt{\frac{L}{C}}, \quad \tau = \sqrt{LC}t$$

which is transformed into the following system:

$$\begin{aligned} \dot{x}_1 &= -\gamma x_1 + x_2(1-u) \\ \dot{x}_2 &= -x_1(1-u) + 1 \end{aligned} \tag{2}$$

where $\gamma = \frac{1}{R}\sqrt{\frac{L}{C}} = 0.35$, or

$$\begin{pmatrix} \dot{x}_1 \\ \dot{x}_2 \end{pmatrix} = \begin{pmatrix} -\gamma & 1-u \\ u-1 & 0 \end{pmatrix} \begin{pmatrix} x_1 \\ x_2 \end{pmatrix} + \begin{pmatrix} 0 \\ 1 \end{pmatrix} \tag{3}$$

For each topology, with $i = 1$ we have $u = 1$ (first topology) and with $i = 2$ we have $u = 0$ (second topology) then the system (3) can be expressed as

$$\dot{\mathbf{x}} = A_i\mathbf{x} + B \tag{4}$$

with

$$A_1 = \begin{pmatrix} -\gamma & 0 \\ 0 & 0 \end{pmatrix},\ A_2 = \begin{pmatrix} -\gamma & 1 \\ -1 & 0 \end{pmatrix},\ B = \begin{pmatrix} 0 \\ 1 \end{pmatrix} \tag{5}$$

The solution of the system (4)–(5) for each topology is given by

$$\mathbf{x}(t) = e^{A_i(t-t_0)}\mathbf{x}(t_0) + \int_{t_0}^{t} e^{A_i(t-\tau)}Bd\tau,$$

for $i = 1, 2$. Or,

$$\mathbf{x}(t) = \phi_i(t-t_0)\mathbf{x}(t_0) + \psi_i(t-t_0) \tag{6}$$

where

$$\phi_i(t-t_0) = e^{A_i(t-t_0)} \quad \text{and} \quad \psi_i(t-t_0) = \int_{t_0}^{t} e^{A_i(t-\tau)}Bd\tau. \tag{7}$$

The system will be controlled by lateral pulse width modulator that provides zero average dynamics on the commutation surface $s(\mathbf{x})$ in a commutation period.

The design for the commutation surface is based on the theory of variable-structure systems with sliding mode [30]. In order to make the output of the system v_o to follow a certain desired signal $v_{ref} > 0$, one can use the ZAD strategy. Setting $x_{1ref} = v_{ref}/V_{in}$ one defines the error surface

$$s(\mathbf{x}) = (x_1 - x_{1ref}) + k_1(x_2 - x_{2ref}) + k_2\int_{kT}^{t}(x_1 - x_{1ref})dt \tag{8}$$

where x_1 and x_2 are the variables we are going to control, x_{1ref} and x_{2ref} the reference signals and k_1, k_2 the constants associated with first order dynamics of the error surface $s(\mathbf{x}(t)) = 0$ given by the commutation surface Eq. (8).

The control lateral pulse sketches (see figure 1) are defined by

- Case $u = \{1, 0\}$

$$u = \begin{cases} 1, & \text{if } kT \le t \le kT + d \\ 0, & \text{if } kT + d \le t \le (k+1)T \end{cases} \tag{9}$$

  In this case d is the time in which the system is in $u = 1$.

- Case $u = \{0, 1\}$

$$u = \begin{cases} 0, & \text{if } kT \le t \le kT + d \\ 1, & \text{if } kT + d \le t \le (k+1)T \end{cases} \tag{10}$$

In this case d is the time in which the system is in $u = 0$.

In both cases, the value of d is called duty cycle. The goal is that there exist a duty cycle that provides zero average dynamic on the commutation surface $s(\mathbf{x})$

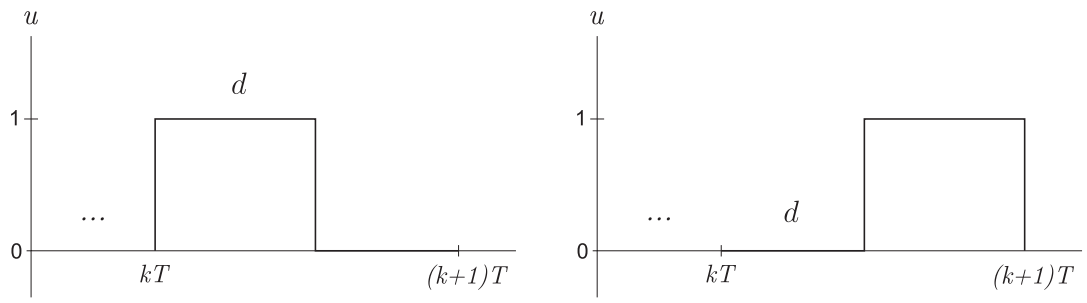

(a) Case $u = \{1, 0\}$. (b) Case $u = \{0, 1\}$.

Figure 1: Control signal u for lateral PWM.

in each sampling period. In (9) and (10), the ZAD strategy determines the duty cycle d and guarantees that the output x_1 follows the reference x_{1ref}. The duty cycle d is calculated using the equation (zero average)

$$\int_{kT}^{(k+1)T} s(\mathbf{x}(t))\, dt = 0 \tag{11}$$

If we want to compute the exact duty cycle in each iteration, it implies solving a trascendental equation which is a serious inconvenient for a physical implementation. To simplify computing we will use a simpler technique.

2.1 Linear approximation of $s(\mathbf{x}(t))$

For this approximation, we assume the following [21]:

1. The commutation surface behaves like a piecewise-linear function.
2. The commutation surface slopes are given by the slopes calculated at the switching instant.

These hypothesis can be easily verified (see figure 2).

Following these considerations, we obtain the duty cycle expression at the instant $[0, T]$ for both control laws.

$$d = \left(1 - \sqrt{\frac{\dot{s}_1 + 2s/T}{\dot{s}_1 - \dot{s}_2}}\right) T \tag{12}$$

The difference between both cases is in the computation of slopes $\dot{s}_1$ and $\dot{s}_2$.

3 Nonlinear dynamics

In this section the nonlinear dynamics of the boost converter are briefly described by the analysis of bifurcation diagrams when key parameters are varied in a convenient range. Later, we show the existence of chaos in the system by Lyapunov

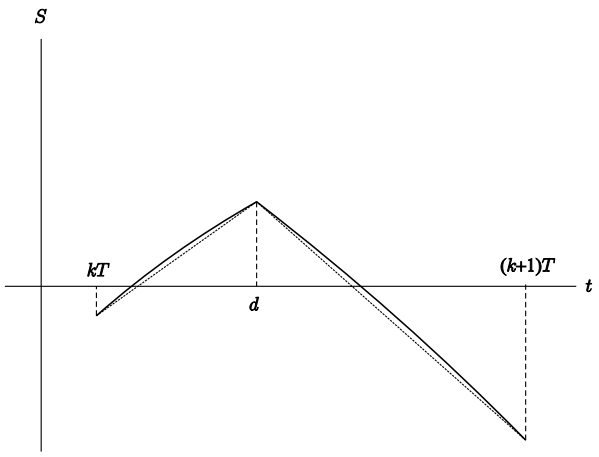

Figure 2: Linear approach of $s(\mathbf{x})$.

exponents. A way to analyze nonlinear phenomena in the boost converter controlled by Lateral PWM and ZAD is by bifurcation diagrams. In the bifurcation diagrams we only consider the behavior of the system in steady state. Now we will show some bifurcation diagrams for x_1, x_2 and d varying parameters k_1 and k_2 using the control signal u for cases $\{1, 0\}$ and $\{0, 1\}$, where the values for x_{1ref} and x_{2ref} are respectively 2.5 and 2.1875.

3.1 Bifurcations analysis with k_1

Neimark Sacker bifurcation (NSB)

Figure 3a shows a bifurcation diagram for x_1 when the control signal is $u = \{1, 0\}$. For this case, we observe a stable periodic orbit which loss stability due to a NSB. Figure 3b shows eigenvalues loci of the Jacobian matrix of the Poincaré map when parameter k_1 is increased and we can appreciate that eigenvalues cross the unit circle being complex conjugates. Neimark-Sacker bifurcation occurs approximatively for $k_1 = -1.9603$. After this bifurcation, the trajectory of the system in the steady state is a torus (quasi-periodic behavior) which, after another change of the bifurcation parameter, can experiment a nonsmooth bifurcation called Border Collision (BC) obtaining a 15-periodic orbit. This bifurcation occurs when the duty cycle is saturated.

Flip bifurcation (FB)

We can observe in Figure 4a a bifurcation diagram for x_1 when the control signal is $u = \{0, 1\}$. Here, we can appreciate a periodic orbit for a wide range of values of k_1. When parameter k_1 is increased, a flip bifurcation occurs, and the steady state of the system goes from a 1-periodic to a 2-periodic orbit. This bifurcation occurs for $k_1 = -1.0656$.

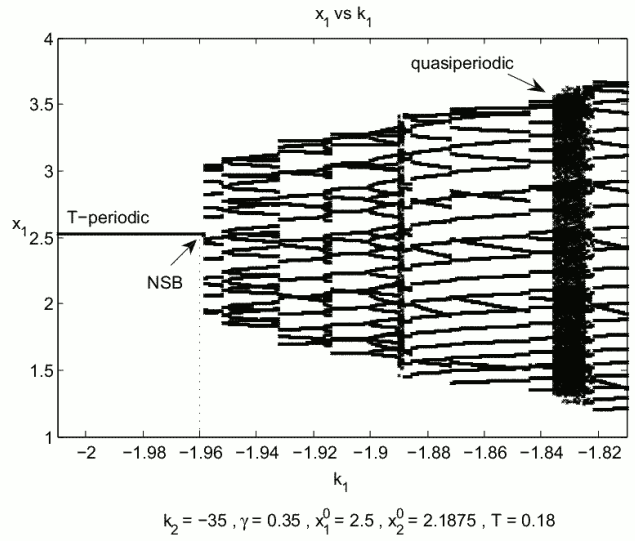

(a) Bifurcation diagram showing a NSB

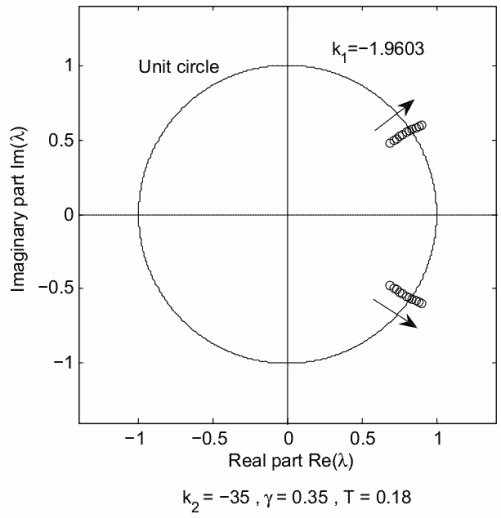

(b) Eigenvalues loci of the Jacobian matrix of the Poincaré map when the parameter k_1 is increased

Figure 3: Neimark Sacker bifurcation. Control $u = \{1, 0\}$

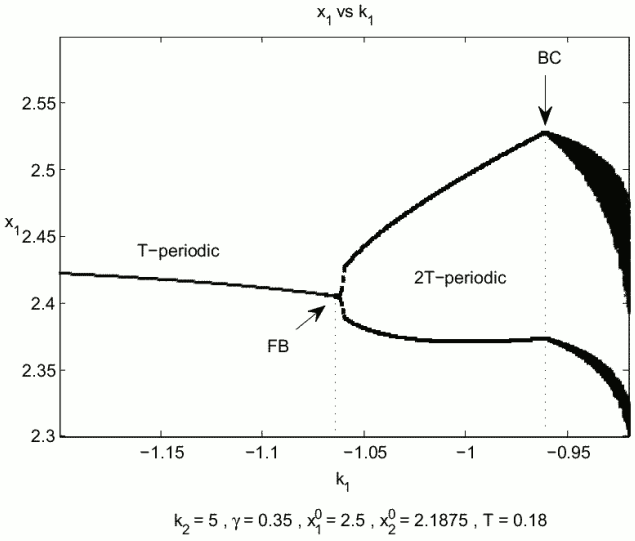

(a) Bifurcation diagram showing a FB

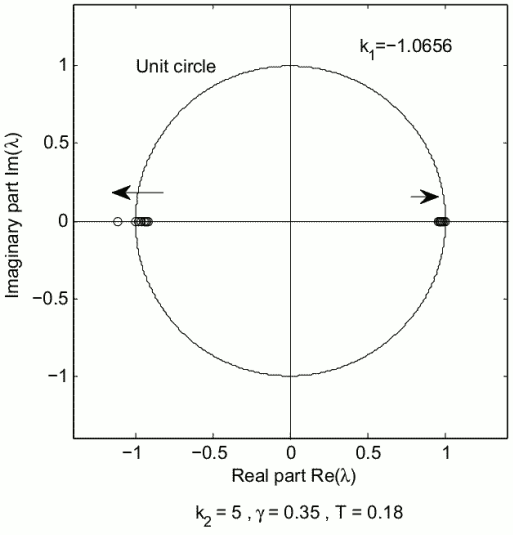

(b) Eigenvalues loci of the Jacobian matrix of the Poincaré map when the parameter k_1 is increased

Figure 4: Flip bifurcation. Control $u = \{0, 1\}$

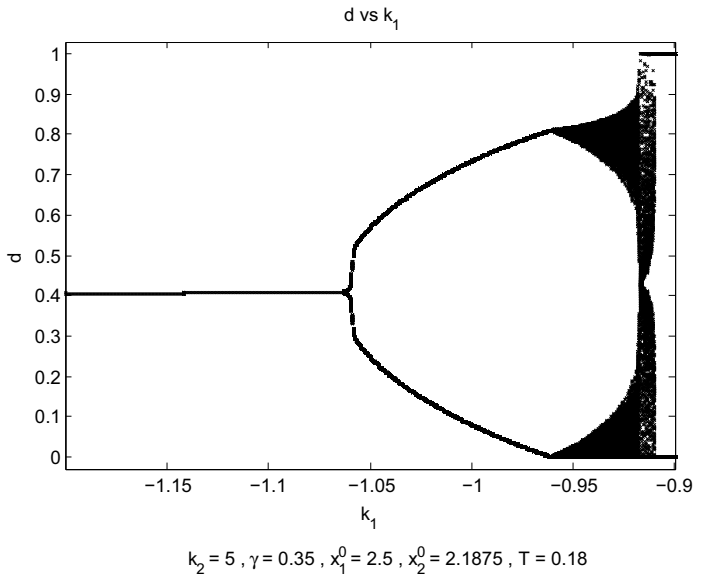

Figure 5: Bifurcation diagram. d vs k_1. Control $u = \{0, 1\}$

As we said for the previous bifurcation, eigenvalues of the Jacobian matrix of the Poincaré map are showed when the parameter k_1 is increased. This parameter varies in $(-1.2, -0.92)$. In Figure 4b results are shown and we can appreciate that eigenvalues cross the unit circle in $(-1, 0)$ deducing that the system presents a FB for $k_1 = -1.0656$. Note that a nonsmooth bifurcation which can be characterized as a BC occur afterwards (this for $k_1 = -0.9618$) and finally the system presents chaotic behavior. If we observe Figure 5 we can see that one of the duty cycles of the 2-periodic orbit is saturated to 0 for $k_1 = -0.9618$. Then, a border collision bifurcation produces chaotic behavior.

3.2 Bifurcation analysis with k_2

In this case, we have a bifurcation diagram for x_1 in a wide range of values of k_2 (see Figure 6) when control law is $u = \{1, 0\}$. Bifurcation diagrams show a stable 1-periodic orbit for values less than $k_2 = -7.1476$ where it loses stability and a 2-periodic orbit is born.

Nonsmooth characteristics for the 2-periodic can be explained observing Figure 7. For values k_2 in the interval $(-7.1476, -7.1406)$ the system presents two non-saturated duty cycles. For the value $k_2 = -7.1406$ one of the duty cycles is saturated in $d = T$ where the 2-periodic orbit remains stable with a saturated duty cycle. When k_2 takes the value of 21.1322 the saturation of the other duty cycle in $d = 0$ appears, obtaining therefore a 2-periodic orbit with both saturated duty cycles.

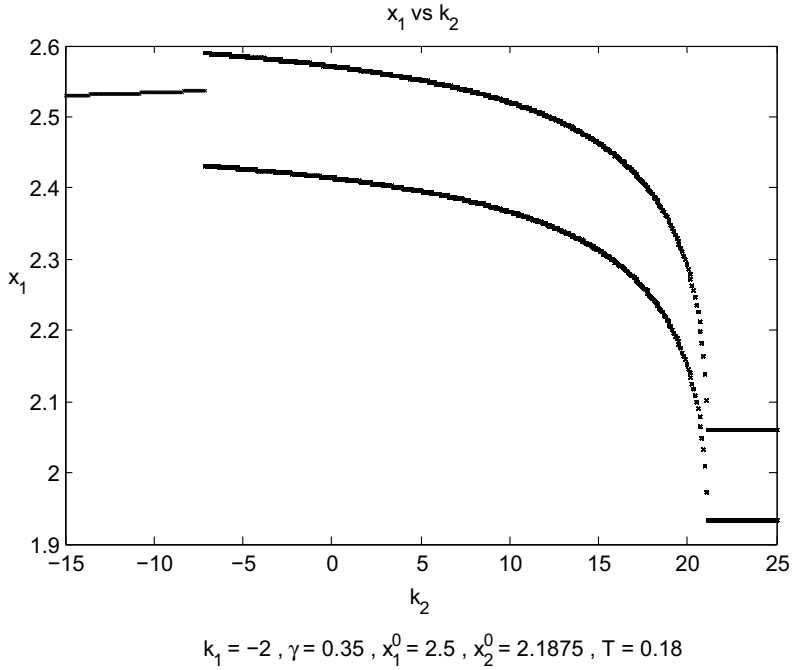

Figure 6: Bifurcation diagram. x_1 vs k_2. Control $u = \{1, 0\}$

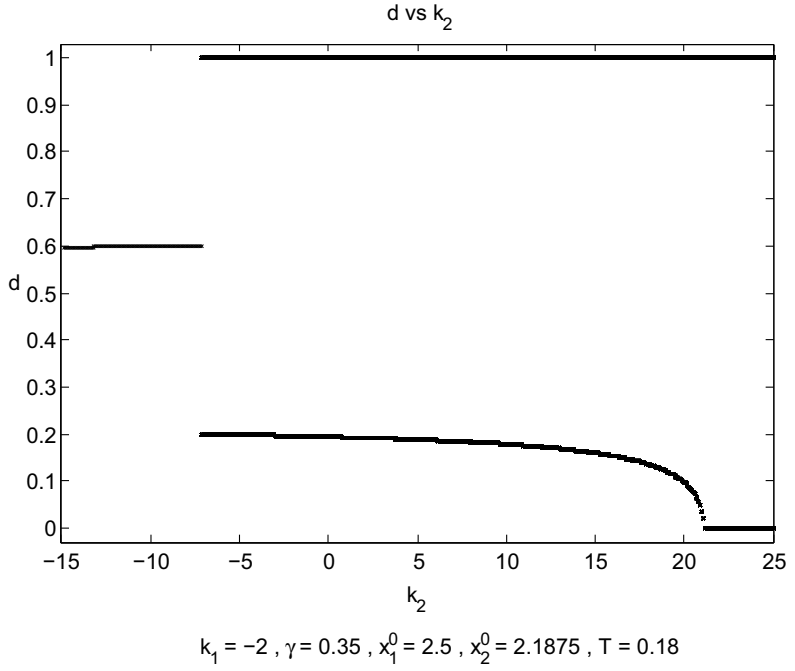

Figure 7: Bifurcation diagram. d vs k_2. Control $u = \{1, 0\}$

3.3 Existence of chaos by Lyapunov exponents

In this section we are going to determine the existence of chaotic behavior in the system using Lyapunov exponents. Lyapunov exponents are a generalization of the characteristic multipliers. They measure the radius of separation of two close orbits in the space state. We will use the Lyapunov exponents to determine the stability of quasi-periodic orbits and the chaotic behavior of the system, since the presence of a positive Lyapunov exponent in a system where their trajectories evolve within a finite zone of the space state guarantees chaotic behavior [6].

In order to calculate the Lyapunov exponents we must consider the solution of the system given by (4) with the ZAD strategy (11) in $[kT, (k+1)T]$. Using (6) and (7) the solution $\mathbf{x}((k+1)T)$ is easily shown to be

$$\begin{aligned}\mathbf{x}((k+1)T) = \phi_2((k+1)T - d_k)\phi_1(d_k)\mathbf{x}(kT) \\ + \phi_2((k+1)T - d_k)\psi_1(d_k) + \psi_2((k+1)T - d_k)\end{aligned} \tag{13}$$

with d_k like in (12). We will express equation (13) as

$$\mathbf{x}(k+1) = \mathbf{P}(\mathbf{x}(k)) \tag{14}$$

On the other hand, $\mathbf{DP}(\mathbf{x})$ is the Jacobian matrix of Poincaré map $\mathbf{P}$, and $v_i(\mathbf{DP}(\mathbf{x}))$ is the i-th eigenvalue of $\mathbf{DP}(\mathbf{x})$. The Lyapunov exponent λ_i associate for every eigenvalue. It is defined as [31]:

$$\lambda_i = \lim_{n\to\infty}\left[\frac{1}{n}\sum_{k=0}^{n}\ln|v_i(\mathbf{DP}(\mathbf{x}(k)))|\right] \tag{15}$$

In Figure 8 we observe the evolution of Lyapunov exponents when the bifurcation parameter k_1 is increased. This figure shows us that in the bifurcation diagram that was showed in Figure 3b for the evaluation range of the bifurcation parameter k_2 when it is varied between -2.01 and -1.81 the system does not present chaotic behavior. Therefore we have quasi-periodicity.

Figure 9 shows the evolution of the Lyapunov exponents when the parameter for bifurcation k_2 is increased. Here, we observe that there is no presence of a positive Lyapunov exponent. Then, the stability of the system when $k_2 \in (-15, 25)$ is verified as it was mentioned in the previous subsection by diagrams 6 and 7.

In Figure 10 we observe the existence of positive Lyapunov exponents in the interval $(-1.0512, -0.9114)$. This can be due to the presence of chaos in this zone. However, Figure 5 shows that in the interval $(-1.18, -0.9618)$ there is no chaotic behavior. This phenomena can be explain by the following:

- Presence of a secondary chaotic atractor with a stable manifold so small that it is not possible to reach it numerically, after the given initial conditions.
- The existence of unstable periodic orbits of sufficiently large periods, which can not be detected numerically, which would not imply presence of chaos.

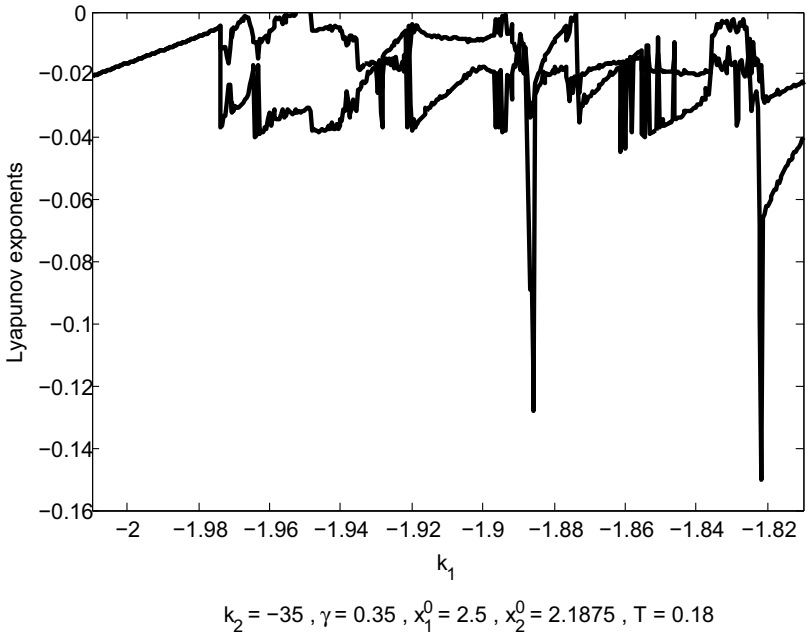

Figure 8: Lyapunov exponents PWML. Control $u = \{1, 0\}$.

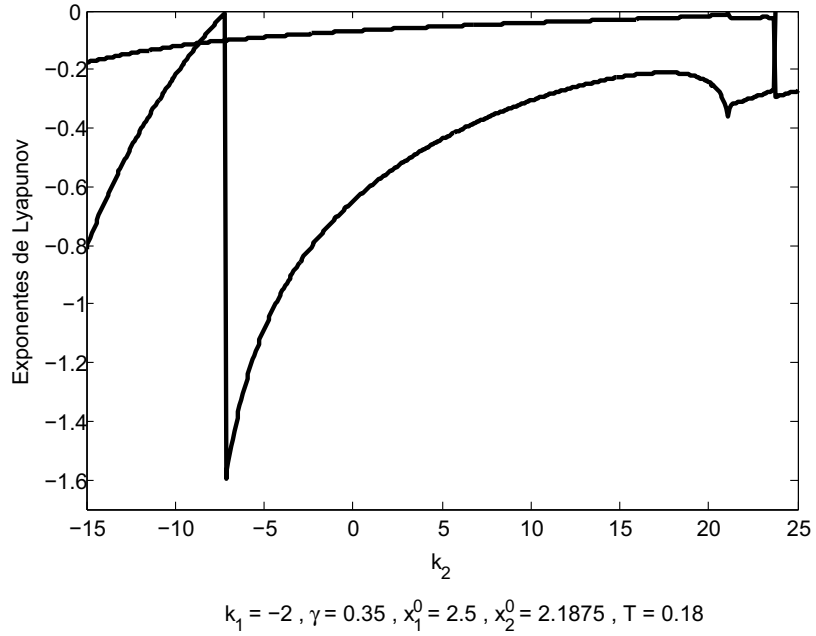

Figure 9: Lyapunov exponents PWML. Control $u = \{1, 0\}$.

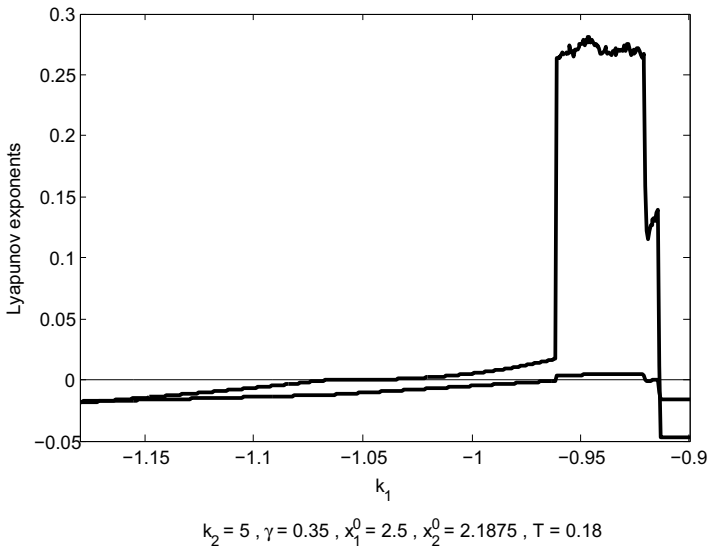

Figure 10: Lyapunov exponents PWML. Control $u = \{0, 1\}$.

4 Chaos control with FPIC

This section describe FPIC technique which is used to stabilise 1-periodic orbits close to the chaotic attractor. In this technique the system is forced to converge to a fixed point. Based on that point, the control strategy is designed. With the use of this strategy, we look for a fixed switching frequency (with zero average on the commutation surface) and a low output error. Considering the duty cycle of the system as the controlled variable, it is enough modify the duty cycle according to

$$d(k) = \frac{d + Nd_{ss}}{N + 1} \tag{16}$$

where $d(k)$ is the duty cycle to be applied, d is the value calculated in (12), d_{ss} is the steady-state duty cycle and N is an arbitrary nonnegative constant.

4.1 FPIC control for the case $u = \{1, 0\}$

For this case, the steady-state duty cycle is $d_{ss} = 0.592672$, considering that the duty cycle is normalized taking values between 0 and 1. According to the value of d_{ss} and the expression calculated in (16) we have bifurcation diagrams for different values of the constant N. Parameter k_1 takes values in the interval $(-2.01, -1.82)$. Figure 11a shows a bifurcation diagram for a value of $N = 1$. The stable 1-periodic orbit occurs for k_1 values less than -1.892, while in Figure 3a 1-periodic orbit occurs for values less than -1.9603.

Now, taking $N = 10$, we can see in Figure 11b that the 1-periodic orbit keeps stable for every value of parameter k_1 in the interval $(-2.01, -1.82)$.

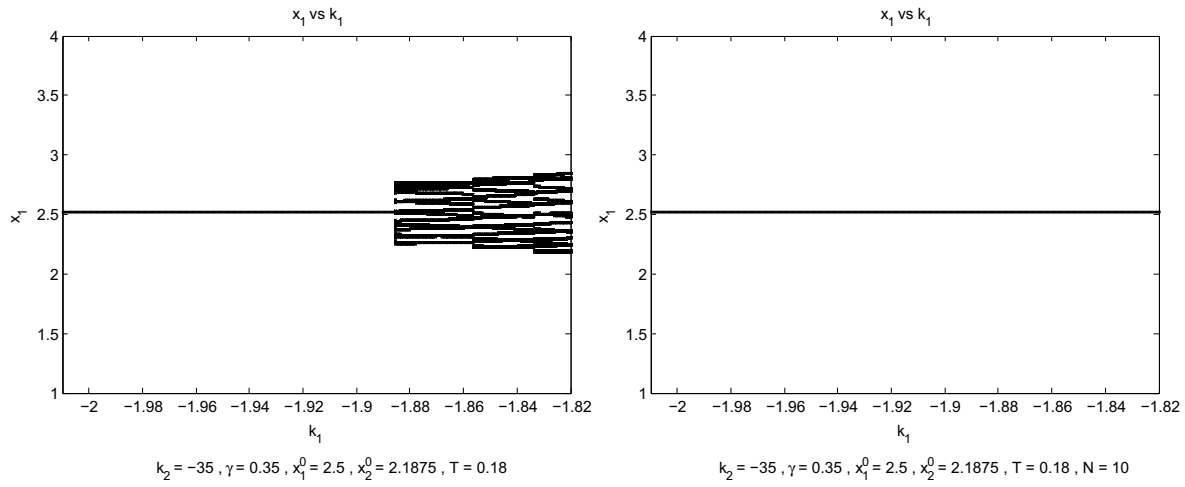

(a) $N = 1$. (b) $N = 10$.

Figure 11: Bifurcation diagram. x_1 vs k_1. FPIC control.

4.2 FPIC control for the case $u = \{0, 1\}$

For this case, the steady state duty cycle is $d_{ss} = 0.392213$. As it was mentioned in the last case, according to the expression (16), we obtained bifurcation diagrams for different values of N. Figure 12 shows bifurcation diagrams for $N = 1$ and $N = 10$. If we compare these diagrams with the ones shown in Figure 4 we can see that the 1-periodic orbit keeps stable for all values of parameter k_1 in the interval $(-1.2, -0.92)$.

The difference from considering $N = 1$ and $N = 10$, is that in the first value of N, x_1 moves away from the reference value, while for $N = 10$, x_1 approaches to the reference value.

5 Chaos control with TDAS

This section describe TDAS technique. This technique looks for the stabilization of unstable periodic orbits. The goal is to feedback a time-delayed variable. Since the variable that induces stability in the system can be associated with the duty cycle, it is possible to derive a new expression for the duty cycle computation in order to stabilize the periodic orbit [26]:

$$d(k) = d + \eta(d(k) - d(k-1)) \tag{17}$$

where $d(k)$ is the duty cycle to be applied, d is the duty cycle obtained in (12), $d(k-1)$ is the duty cycle of the last iteration and η is the feedback constant.

5.1 TDAS control for the case $u = \{1, 0\}$

In Figure 13 we observe the bifurcation diagrams for x_1 when we apply TDAS control technique for values of η as 0.2 and 0.4 respectively. In Figure 13a we can

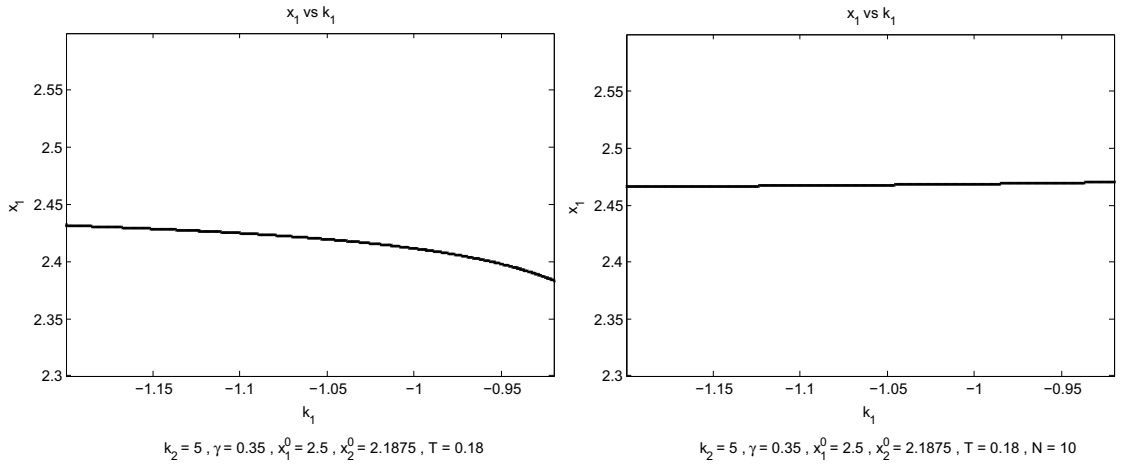

(a) $N = 1$. (b) $N = 10$.

Figure 12: Bifurcation diagram. x_1 vs k_1. FPIC control.

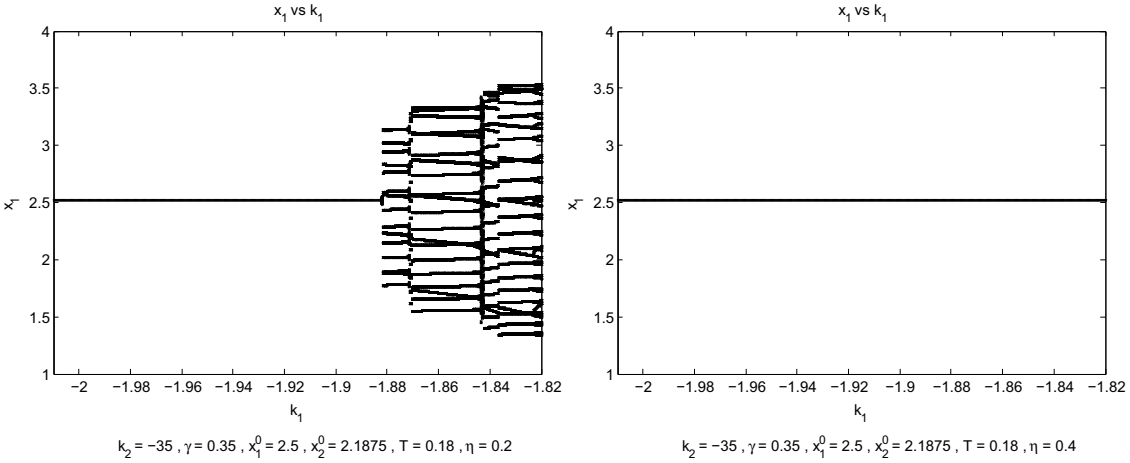

(a) $\eta = 0.2$. (b) $\eta = 0.4$.

Figure 13: Bifurcation diagram. x_1 vs k_1. TDAS control.

appreciate that the 1-periodic orbit keeps stable for values of parameter k_1 less than -1.8824. When $\eta = 0.4$ we can see in Figure 13b that this technique has a better performance for this value of the feedback constant, since it stabilizes the 1-periodic orbit in the interval $(-2.01, -1.82)$. Regarding regulation, the maximum regulation error is 0.8%. Therefore, in these cases this technique shows good performance in the sense that it maintains stable the periodic orbit for a wide range of values of k_1.

When we apply the FPIC and TDAS techniques when $k_2 = -35$, and $k_2 \in (-2.01, -1.82)$ we see good performances since they stabilize the 1-periodic orbit and the maximum regulation error is less than 1%. A difference between both techniques is that when one stabilize the orbit with FPIC, it is only necessary to increase the value of parameter N, whereas with TDAS, the feedback constant

can take positive and negative values.

5.2 TDAS control for the case $u = \{0, 1\}$

Figure 14 shows the bifurcation diagrams of x_1 when the feedback constant η is -0.01 and -0.02 respectively. In the diagram of Figure 14a we observe that this technique obtains a good performance since the presence of chaos disappears and the 1-periodic orbit keeps stable for values $k_1 < -0.951$. If $\eta = -0.02$, the diagram of Figure 14b shows that the 1-periodic orbit keeps stable for all the evaluation range of the bifurcation parameter k_1 obtaining a regulation error of 8%.

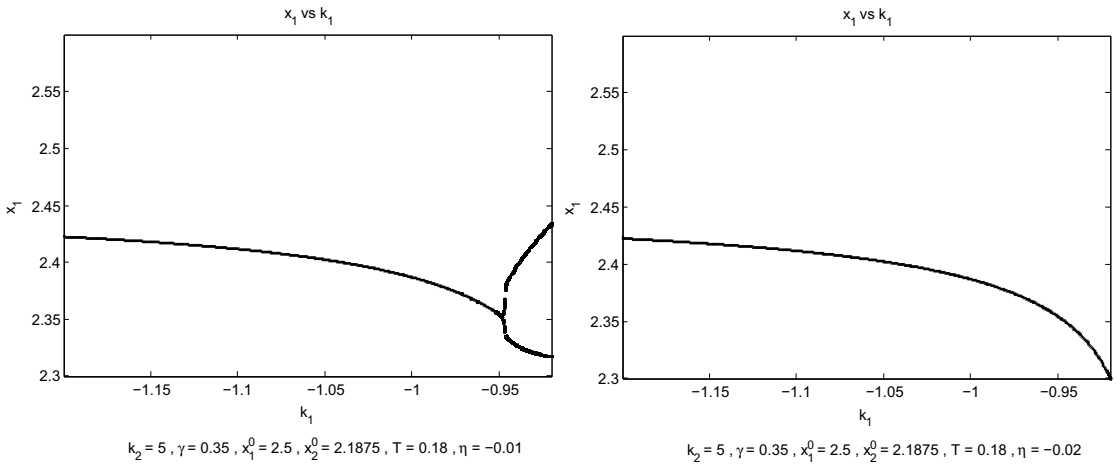

(a) $\eta = -0.01$. (b) $\eta = -0.02$.

Figure 14: Bifurcation diagram. x_1 vs k_1. TDAS control.

6 Conclusions

- The expression of the duty cycle was calculated when the system is controlled with PWML and ZAD by a linear approach of the commutation surface.
- The system presented two smooth bifurcations: Neimark - Sacker and flip and a nonsmooth bifurcation characterized like border collision.
- Numerical calculation of the stability by Lyapunov exponents was done, which allows to conclude the presence of chaos in the system.
- FPIC technique had a better performance than TDAS technique for both possible cases of the control signal u, in the sense that it stabilizes the 1-periodic orbit. For FPIC the stabilization of the 1-periodic orbit is obtained for a greater rank of values of parameters k_1 and k_2, and also better regulation is obtained.

References

[1] Deane, J.H.B. and Hamill, D.C. Instability, subharmonics, and chaos in power electronic systems. IEEE Power Electronics Society, pp. 260–268, (1990).

[2] Deane, J.H.B. and Hamill, D.C. Analysis, simulation and experimental study of chaos in the buck converter. Proc IEEE Power Electronics Specialists Conference (PESC'90), San Antonio, TX, pp. 491–498, (1990).

[3] Gerard Olivar. Chaos in the Buck Converter. PhD Tesis, UPC, (1997).

[4] Chan, Willian C. Y. and Tse, C. K. Bifurcations in current-programmed DC/DC buck switching regulators-conjecturing a universal bifurcation path. International Journal of Circuit Theory and Applications, Vol. 26, pp. 127–145, (1998).

[5] Tse, C.K. and Lai, Y.M. Control of bifurcation in current-programmed DC/DC converters: a reexamination of slope compensation. Circuits and Systems, Vol. 1, pp. 671–674, (2000).

[6] Banerjee, Soumitro and Verghese, George. Nonlinear Phenomena in Power Electronics: Attractors, Bifurcations, Chaos, and Nonlinear Control. Wiley-IEEE Press, (2001).

[7] Tse, C.K. and di Bernardo, M. Complex behavior in switching power converters. IEEE, pp. 768–781, (2002).

[8] Maity, Somnath and Bhattacharya, Tapas K. and Banerjee, Soumitro. Experimental Study of Chaos and Bifurcation in the Buck Converter. National Conference on Nonlinear Systems & Dynamics, (2005).

[9] Taborda, J.A. and Angulo, F. and Olivar, G. Smooth bifurcations in 3D-parameter space of Digital-PWM Switched Converter. Circuits and Systems (LASCAS), 2011 IEEE, pp. 1–4, (2011).

[10] Deane, J.H.B. Chaos in a Current-Mode Controlled Boost dc-dc. IEEE Trans. Circuit Syst. I, Vol. 39, pp. 680–683, (1992).

[11] Zafrany, I. and Ben-Yaakov, S. A chaos model of subharmonic oscillations in current mode PWM boost converters. Proc IEEE Power Electronics Specialists Conference, pp. 1111–1117, (1995).

[12] Fossas E. and Olivar G. Study of Chaos in the Buck Converter. IEEE Trans. Circuits Syst. I, pp. 13–25, (1996).

[13] Chan, W. and Tse, C. Study of Bifurcations in Current-Programmed DC/DC Boost Converters: From Quasi-Periodicity to Period-Doubling. IEEE Trans. Circuits Syst. I., pp. 1129–1142, (1997).

[14] di Bernardo M., Garofalo F., Glielmo L. and Vasca F. Switchings, Bifurcations, and Chaos in DC/DC Converters. IEEE Trans. Circuits Syst. I, pp. 133–141, (1998).

[15] Banerjee S and Chakrabarty, K. Nonlinear Modeling and Bifurcations in the Boost Converter. IEEE Trans. Power Electr., pp. 252–260, (1998).

[16] El Aroudi, A., Benadero, L., Toribio, E. and Olivar, G. Bifurcation and Chaos from Torus Breakdown in a PWM Voltage-Controlled DC-DC Boost Converters. IEEE Trans. Circuits Syst. I., pp. 1374–1382, (1999).

[17] Cheng, K.W.E. and Liu, M. and Wu, J. and Cheung, N.C. Study of Bifurcation and Chaos in the Current-Mode Controlled Buck-Boost DC-DC Converter. Proc IEEE Industrial Electronics Society (IECON'01), Denver, CO, pp. 838–843, (2001).

[18] Kocewiak, Lukasz and Bak, Claus Leth and Munk-Nielsen, Stig. Bifurcations and Chaos in a Pulse Width Modulation Controlled Buck Converter. Proceedings of the 6th EUROSIM Congress on Modelling and Simulation, (2007), pp. 1–6.

[19] Angulo, Fabiola and Fossas, Enric and Olivar, Gerard. Transition From Periodicity To Chaos In A Pwm-Controlled Buck Converter With Zad Strategy. Int. J. Bifurcation and Chaos, Vol. 15, No. 10, pp. 3245–3264, (2009).

[20] Fossas, E and Hogan, S. J. and Seara,T. M. Two-parameter bifurcation curves in power electronic converters. Int. J. Bifurcation and Chaos, Vol. 19, pp. 349–357, (2009).

[21] Angulo Fabiola. Análisis de la dinámica de convertidores electrónicos de potencia usando PWM basado en promediado cero de la dinámica del error (ZAD). Tesis de doctorado, UPC. Mayo de (2004).

[22] Fossas E., Griñó R. and Biel D. Quasi-sliding control based on pulse width modulation, zero average and the L_2 norm. In Advances in Variable Structure System, Analysis, Integration and Applications. Ed. World Scientific. (2001), pp. 335–344.

[23] Cevantes, I. and Alvarez-Ramirez, J. A simple chaos control strategy for DC-DC power converters. Industrial Electronics Society, Vol. 1, pp. 193–198, (2004). IECON 2004.

[24] Pyragas, K. Continuous control of chaos by self-controlling feedback. Physics Letters, Vol. A, No. 170, pp. 421–428, (1992).

[25] Angulo F. Burgos J.E. and Olivar G. Chaos Stabilization with TDAS and FPIC in a Buck Converter controlled by Lateral PWM and ZAD. Mediterranean Conference on Control and Automation, (2007).

[26] Angulo, F. Fossas, E. Olivar, G Técnica ZAD Aplicada a un Convertidor Buck: Análisis de Estabilidad y de Transición al Caos. Revista Iberoamericana de Automática e Informática Industrial, Vol. 2, No. 4. October (2005), pp. 25–35.

[27] Angulo F. Fossas E. and Olivar G. Stabilization of Chaos with FPIC: Application to ZAD-Strategy Buck Converters. 16th IFAC World Congress, Prague, (2005).

[28] Angulo F. Olivar G. Taborda J. A. and Hoyos, F. E. Nonsmooth dynamics and FPIC chaos control in a DC-DC ZAD-strategy power converter. Proceeding of the VI EUROMECH Nonlinear Dynamics Conference ENOC, Saint Petersburg, Russia, (2008).

[29] Fossas, E. and Zinober, A. Adaptive Tracking Control of Nonlinear Power Converters. Proceedings IFAC Workshop on Adaptation in Control and Signal Processing, Connobio, Italia, pp. 264–266, (2001).

[30] Carpita, M. and Marchesoni, M. and Oberti, M. and Puglisi, L. Power conditioning system using sliding model control. Power Electronics Specialists Conference (PESC'88 Record), 19th Annual IEEE, Kyoto, Japan, pp. 626–633, (1988).

[31] Parker T.S. and Chua L.O. Practical numerical algorithms for chaotic systems. Springer Verlag, New York. (1989). pp. 66–81.

Authors' address

Andrés Amador — Departamento Ciencias Naturales y Matemáticas, Pontificia Universidad Javeriana Cali, Cali-Colombia

e-mail: afamador@javerianacali.edu.co

Simeon Casanova — Departamento de Matemáticas y Estadística, Universidad Nacional de Colombia, Manizales-Colombia

e-mail: scasanovat@unal.edu.co

Julián Hurtado — Departamento de Matemática, Universidad Autónoma de Occidente, Cali-Colombia

e-mail: jhurtado@uao.edu.co

Gerard Olivar — Departamento de Ingeniería Eléctrica, Electrónica y Computación, Universidad Nacional de Colombia, Manizales-Colombia

e-mail: golivart@unal.edu.co